Pseudogap and weak multifractality in 2D disordered Mott charge-density-wave insulator

Jianhua Gao,[†] Jae Whan Park,[†] Kiseok Kim,[‡] Sun Kyu Song,[†,‡] Hae Ryong Park,[†,‡] Jhinhwan Lee,[†] Jewook Park,[†] Fangchu Chen,[¶,§] Xuan Luo,[¶] Yuping Sun,[¶,‖,⊥] and Han Woong Yeom[*,†,‡]

†*Center for Artificial Low Dimensional Electronic Systems, Institute for Basic Science (IBS), Pohang 37673, Korea*

‡*Department of Physics, Pohang University of Science and Technology, Pohang 37673, Korea*

¶*Key Laboratory of Materials Physics, Institute of Solid State Physics, Chinese Academy of Sciences, Hefei 230031, People's Republic of China*

§*University of Science and Technology of China, Hefei 230026, People's Republic of China*

‖*High Magnetic Field Laboratory, Chinese Academy of Sciences, Hefei 230031, People's Republic of China*

⊥*Collaborative Innovation Centre of Advanced Microstructures, Nanjing University, Nanjing 210093, People's Republic of China*

E-mail: yeom@postech.ac.kr

A list of the main contents

- Supplementary Note 3: Domain boundaries in the Se substituted 1 T-TaS_2
- Supplementary Note 4: STS spectra in the Se substituted 1 T-TaS_2
- Supplementary Note 5: STS spectra from the CDW maxima and minima
- Supplementary Note 6: DFT calculation of the electronic states of T-TaS_2 and 1 T-$TaS_{2-x}Se_x$
- Supplementary Note 7: Spatial fluctuation of the electronic states
- Supplementary Note 8: Multifractal spectrum $f(\alpha)$
- Supplementary Note 9: The local electronic properties of 1 T-TaSSe

Supplementary Note 1: Morphology of the Se substituted 1 T-TaS_2

Figure S1 (a) shows a typical STM topographic image with atomic resolution taken at 4.3 K with the scanning area of 16×16 nm^2 at tunneling bias V_s = - 6 mV and tunneling current I_t = 400 pA. The long-range ordered CDW superstructure is evident, and the bright contrast corresponds to the CDW maxima of each David star cluster, with the S and Se atoms randomly arranged. Figure S1 (b) indicates the Fourier transformation (FFT) of the topography image (a). The FFT image displays strong CDW peaks with $\sqrt{13} \times \sqrt{13}$ superstructure and their higher order peaks, which rotate counterclockwise by 13.9° from the primitive atomic lattice 1 T-TaS_2.[1,2] The David star unit cells form hexagonal lattice, with the corresponding Brillouin zone denoted by the red solid lines, and one 1×1 unit cell marked by red dash lines. Figure S1 (c) displays a STM topographic image with the scanning area of 40×40 nm^2 (tunneling bias V_s = + 800 mV and tunneling current I_t = 50 pA). Figure S1 (d) indicates the FFT image of the topography image (c). The statistics analysis was performed on several tens of line profiles for different images, and three typical

of them are shown in Figure S1 (e). The extracted periodicity of the CDW superstructure is about 1.24 ± 0.01 nm, which is larger than that of pristine 1*T*-TaS_2 (1.21 nm) due to the larger atomic radius of Se. Figure S1 (f) displays the STM topographic image within a larger area of 60×60 nm^2 at V_s = 800 mV and I_t = 50 pA. The image includes a few different domains, with two different domains by a 30 rotation between them. The domain boundaries are marked by white lines. Figure S1 (g) denotes the FFT image of image (f), in which two sets of the CDW order patterns can be observed, corresponding to the two different domain orientations.

Supplementary Note 2: Different brightness contrasts of the Se substituted 1*T*-TaS_2

Figure S2 (a) - (p) show the series of topographic images and their corresponding FFT images. The topographic images were acquired over a given area of 24×24 nm^2 at different bias, as indicated in the images. The hexagonal pattern of the CDW vector can be clearly observed from the FFT images, identifying that the long-ordered CDW structure is formed at low temperature for the case of 1*T*-TaSSe (S:Se ratio close to 1:1), which is very similar to that of 1*T*-TaS_2. However, in contrast to the case of 1*T*-TaS_2, these topographic images exhibits different unitcell-by-unitcell contrasts, which was related to the different local Se concentration within the CDW unit cells.[3] These unitcell-by-unitcell contrasts also depend strongly on the scanning bias as shown in the figure, indicating a strong electronic effect. The relative brightness in each image are classified into four different groups of bright, medium, dim and dark (Figure S3), as marked by white, green, dark blue and light blue circles in the images, respectively. As can be seen from this series of images, this brightness variation is not consistent for the images with different bias.

Supplementary Note 3: Domain boundaries in the Se substituted $1\,T$-TaS_2

Figure S4 display the STM topographic images with different scanning parameters acquired from the different sample locations, in which the $1\,T$-TaSSe surface splits into different domains separated by the domain boundaries. The topographic images consist of a few different domains and the domain boundaries are marked by the white lines in the images. The long-range ordered CDW superstructure is preserved within the single domain region.

Supplementary Note 4: STS spectra in the Se substituted $1\,T$-TaS_2

In order to investigate the electronic structure variation over different CDW unit cells, scanning tunneling spectroscopy (STS) measurements were performed over many different unit cells. Note that the topographic image in Figure S5 (a) shows the different brightness for the CDW maxima over neighboring unit cells, which indicates different Se concentration and/or configuration within each unit cell. Figure S5 (b)-(d) shows the typical dI/dV spectra on CDW maxima of different unit cells, as marked in Figure S5 (a). These spectra are collected into groups according to the topographic contrasts of unit cells as classified in Figure S3. The thick (thin) solid lines correspond to the averaged (individual) dI/dV spectra on a given group of unit cells with similar contrasts. The individual spectra within a group show substantially larger variation between unit cells than those of pristine $1\,T$-TaS_2 case.[1] However, the averaged spectra from different contrast groups have little difference, resembling similar spectral features. These findings indicate that the unitcell-by-unitcell variation of the spectra has a random character and is not systematically governed by the topographic contrasts. The topographic contrasts are respected to be related to the local Se concentration/configuration. Therefore, we can conclude that the spectra feature are not correlated

with the local Se concentration (see below).

Supplementary Note 5: STS spectra from the CDW maxima and minima

More detailed spatially-resolved STS measurements were performed simultaneously with the topographic image, as shown in Figure S6 (a) for a smaller area over about nine CDW unit cells. Figure S6 (b) and (c) display the dI/dV spectra from the CDW maxima (central atoms of David star clusters) and minima regions, respectively. The spectra from the maxima (minima) have similar main spectral features but with some intensity variation as discussed above. Several peak features locating at around +520 and -440, +240 and -168, + 64 and -72 meV can be observed, corresponding to the CDW gap edge, Mott and pseudogap states, respectively.

Supplementary Note 6: DFT calculation of the electronic states of T-TaS_2 and 1T-$TaS_{2-x}Se_x$

The theoretical DOS of 1T-TaS_2 in Figure S7 (a) is in good agreement within 0.1 eV with the experimental dI/dV (averaged) spectra. The Mott gap with upper and lower Hubbard states at 150 and -150 meV and the CDW gap with edges at -317 and 364 meV are consistent qualitatively between the calculation and the experimental results. The DOS of the lowest-energy 1T-TaSSe structure (1:1 concentration of S:Se) with $\sqrt{13}\times\sqrt{13}$ periodic boundary condition in Figure S7 (b), however, is not consistent with the experimental dI/dV spectra of disordered 1T-TaSSe sample. In a recent paper, the origin of the disordered phase with different brightness contrast in STM images was directly related to the Se concentration of a single David star cluster through the comparison between local dI/dV spectra and theoretical DOS of the lowest-energy configurations for given Se concentrations.[3] This calculation is well

reproduced here as shown in Figure S7 (c). Considering a simple binomial distribution, the integrated probability of the Se concentration between 0.77 (10 Se atoms in a single David star) and 1.23 (16 Se atoms in a single David star) is 95 %. Within this range, the DOS of lowest-energy configurations are not significantly changed in our calculations. This DOS should be similar to what is shown in Figure S7 (b) with two well defined peaks at below and above the Fermi energy. The LHB state should be shifted down to about -300 meV, which is well localized on each CDW maxima. These characteristic features are not reproduced at all in the present experiment. In fact, the experimentally observed spectra bear little resemblance with the calculated DOS of any given concentration. These discrepancy clearly indicates that the electronic structure of the disordered 1 T-TaSSe can not be described by the DFT+U calculations for the periodic structure of a given concentration and a given S-Se configuration, due to the electron correlation and the disorder effect. As shown below, the atomic configurations (positions of substituted Se atoms) are as important as the Se concentration or configuration for the electronic structure of 1 T-$TaS_{2-x}Se_x$.

Supplementary Note 7: Spatial fluctuation of the electronic states

Figure S8 (a)-(f) display the LDOS maps over a scanning area of 24×24 nm^2 at different scanning bias. The CDW superstructure patterns are clearly seen from all the LDOS maps, but the electronic states have obvious fluctuation between CDW unit cells, and this variation is randomly disordered. We estimate the spatial fluctuation of the electronic states along the dashed lines in the images. The amplitude of this fluctuations is about 20-40 % of the average LDOS values, as shown in Figure S8 (g).

Supplementary Note 8: Multifractal spectrum $f(\alpha)$

Based on the theoretical predictions, the critical states are expected to represent the multifractal spatial structure, which is related to the scale-invariant nature of the wave function. The multifractal structure is usually described by analysis of the self-similarity through the singularity spectrum $f(\alpha)$. Physically, $f(\alpha)$ describes all the fractal dimensions that share a common exponent α in a spatial pattern, where the eigenfunction intensity satisfy $|\Psi^2(\vec{r})| \sim L^{-\alpha}$.[4–6] A variety of techniques have been developed to calculate $f(\alpha)$. Here, the multifractal spectra is calculated by following the method developed in Ref.[6] The spatial probability distribution of the wave function

$$P_q = \int |\Psi(r)|^{2q} \, d^d r L^{-\tau_q} \tag{1}$$

The multifractal spectrum can be achieved by the Legendre transform

$$f(q) = \alpha q - \tau(q) \tag{2}$$

$$\alpha = \frac{d\tau(q)}{dq} \tag{3}$$

According to the method proposed by Chahabra and Jensen, the multifractal spectra $f(\alpha)$ can be calculated as follows

$$f(q) = \lim_{L\to 0} \frac{\sum_i \mu_i(q,L) \log[\mu_i(q,L)]}{\log L} \tag{4}$$

$$\alpha(q) = \lim_{L\to 0} \frac{\sum_i \mu_i(q,L) \log[P_i(L)]}{\log L} \tag{5}$$

Figure 4 shows the $f(\alpha)$ calculated by using the box-counting technique[5,6] for the LDOS maps at different energies. For all the energies, the $f(\alpha)$ spectra exhibit finite width and

parabolic shape, with the maximum values locating at the position of $\alpha_0 = d + \epsilon$, where $d = 2.0$ and $\epsilon \ll 1$. The multifractal spectra exhibit parabolic shape together with the maximum position at $d + \epsilon$ with $\epsilon \ll 1$, demonstrating that the LDOS exhibits the weak multifractal behavior.[4] The multifractality would be strong in non-interaction systems but be suppressed in interacting systems as the present case. The weak multifractal behavior together with the Gaussian distribution identify the disordered extended states as expected in the two-dimensional electronic systems.

Supplementary Note 9: The local electronic properties of 1*T*-TaSSe

Figure S9 shows the comparasion of the local point STS spectra data between the Ref[3] and (b) our present data. As shown here, we can also collect a set of point STS data, which reproduces most of the previous data. The previous focuses on the STS spectral variation of a few individual CDW units selected but our present work systematically analyze the global spectral change in a much larger number of CDW units. Note also that the previous work neglected spectral features near the Fermi energy, which would be related to the pseudogap discussed in the present work (arrows).

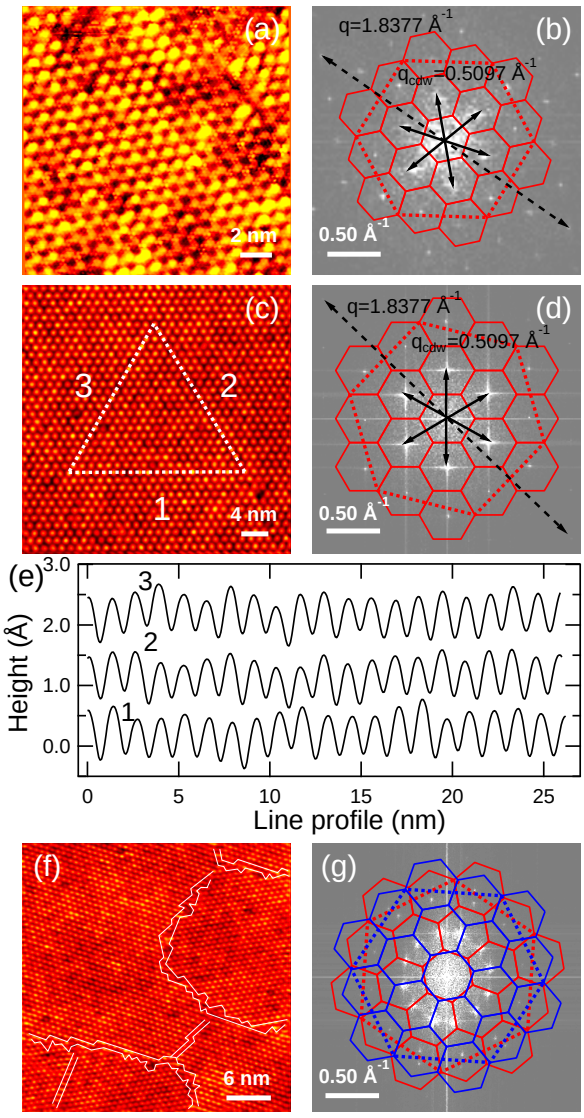

Figure 1: (a) STM topographic image with atomic resolution taken from the 1 T-TaSSe surface over the scanning area of 16×16 nm^2 within a single domain at V_s = -6 mV and I_t = 400 pA. (b) The corresponding Fourier transformation (FFT) image. The hexagons in solid and dashed lines correspond to the first Brillouin zone of the $\sqrt{13} \times \sqrt{13}$ R13.9 CDW structure and 1×1 unit cell, respectively. (c) STM topographic image with the scanning area of 40×40 nm^2 within a single domain at V_s = 800 mV and I_t = 50 pA. (d) The corresponding Fourier transformation (FFT) image. (e) The line profile of the CDW clusters as marked by the white lines in (c), the periodicity of the CDW unit cells is 1.24 ± 0.01 nm. (f) Similar STM image taken across different domain regions with an area of 60×60 nm^2 at V_s = 800 mV and I_t = 50 pA. The domain boundaries are marked by the white lines. (g) The FFT image of (f), in which two sets of $\sqrt{13} \times \sqrt{13}$ R13.9 CDW orders coexist, represented by red and blue lines, respectively. The two sets of CDW orders correspond to the two rotational domains.

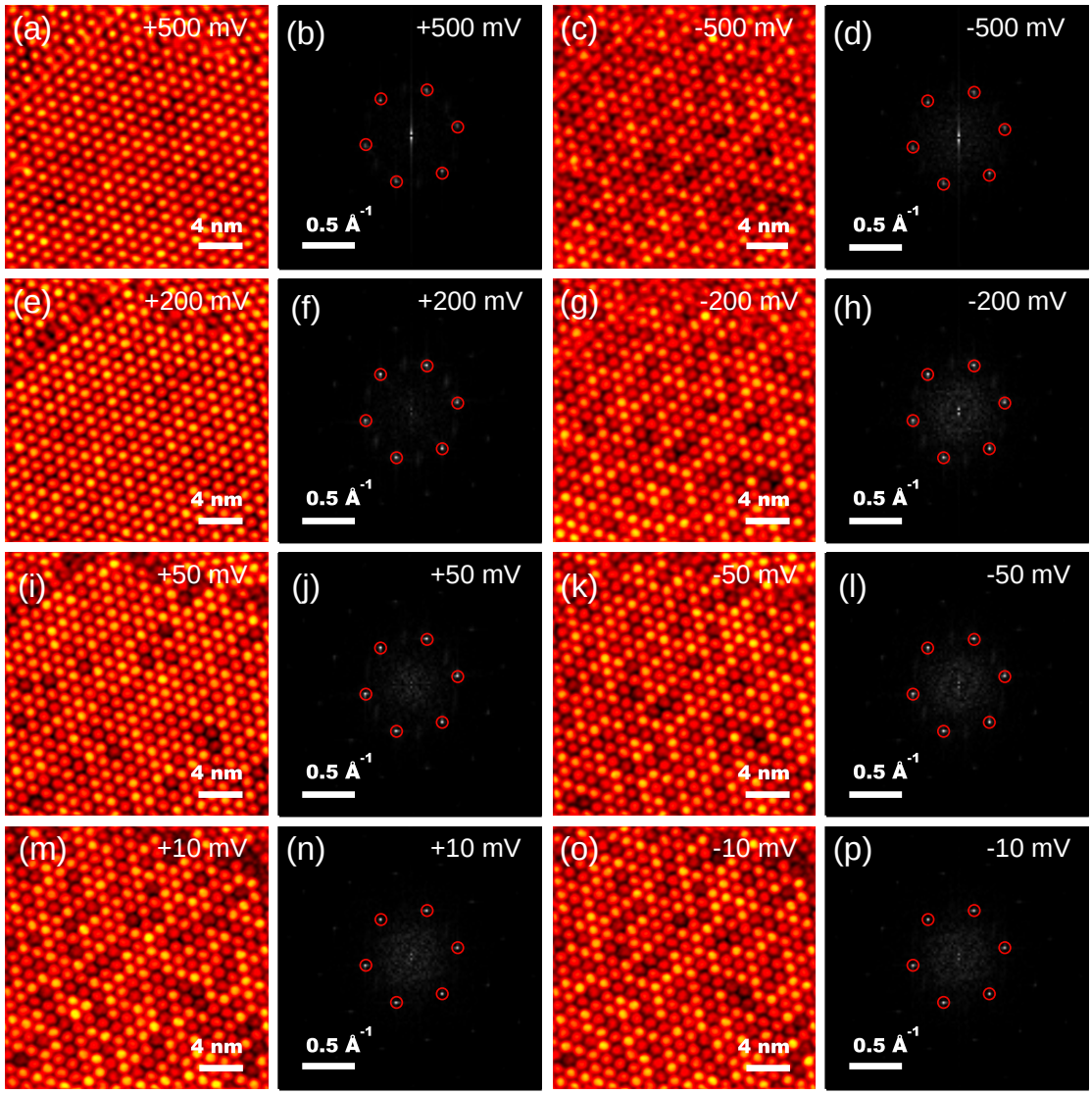

Figure 2: The STM topographic images of the 1 T-TaSSe surface taken over the scanning area of 24×24 nm^2 at various sample bias, and their corresponding FFT images. (a-b) V_s = + 500 mV, I_t = 50 pA; (c-d) V_s = - 500 mV, I_t = 50 pA; (e-f) V_s = + 200 mV, I_t = 50 pA; (g-h) V_s = - 200 mV, I_t = 50 pA; (i-j) V_s = + 50 mV, I_t = 50 pA; (k-l) V_s = - 50 mV, I_t = 50 pA; (m-n) V_s = + 10 mV, I_t = 50 pA; (o-p) V_s = -10 mV, I_t = 50 pA, as indicated in the images.

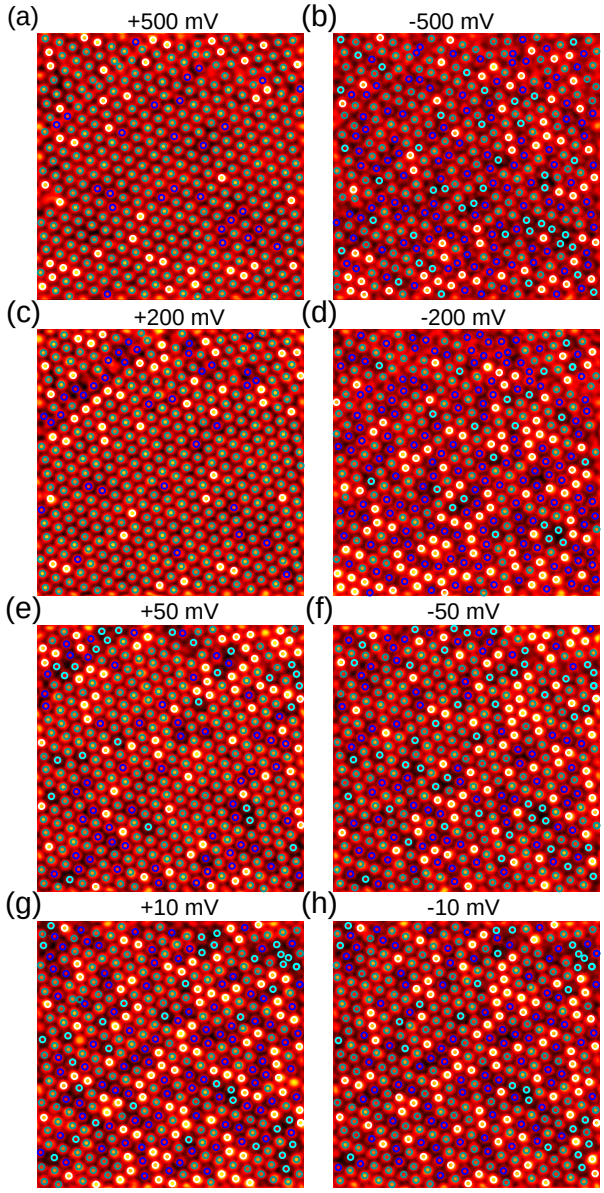

Figure 3: The STM topographic images of the 1 T-TaSSe surface with the same scanning area and scanning condition as those in Figure S2. (a) V_s = + 500 mV, I_t = 50 pA; (b) V_s = - 500 mV, I_t = 50 pA; (c) V_s = + 200 mV, I_t = 50 pA; (d) V_s = - 200 mV, I_t = 50 pA; (e) V_s = + 50 mV, I_t = 50 pA; (f) V_s = - 50 mV, I_t = 50 pA; (g) V_s = + 10 mV, I_t = 50 pA; (h) V_s = -10 mV, I_t = 50 pA, as indicated in the images. The unit cells are classified into four different groups according to the different topographic brightness. The bright, medium, dim and dark contrasts were represented by white, green, dark blue and light blue color circles, respectively.

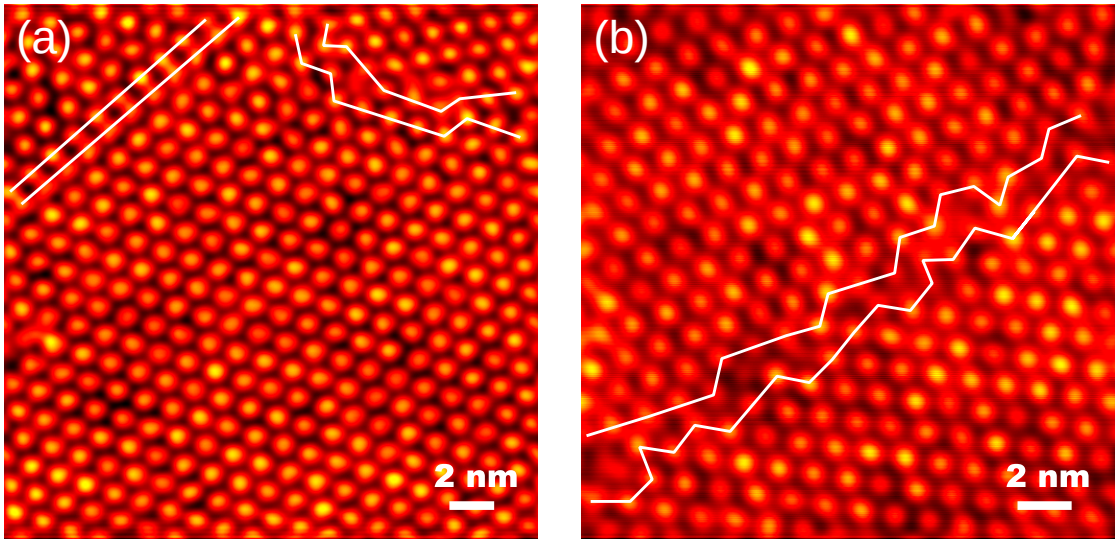

Figure 4: The STM topographic images of 1T-TaSSe with different domains. The domain walls are marked by the white lines as shown in the images. (a) The STM topographic image at the scanning area of 24 $\times$ 24 nm^2, with the scanning parameter at $V_s = +$ 500 mV and $I_t = 50$ pA. (b) The STM image at the scanning area of 20 $\times$ 20 nm^2, with $V_s = +$ 1.20 V and $I_t = 50$ pA.

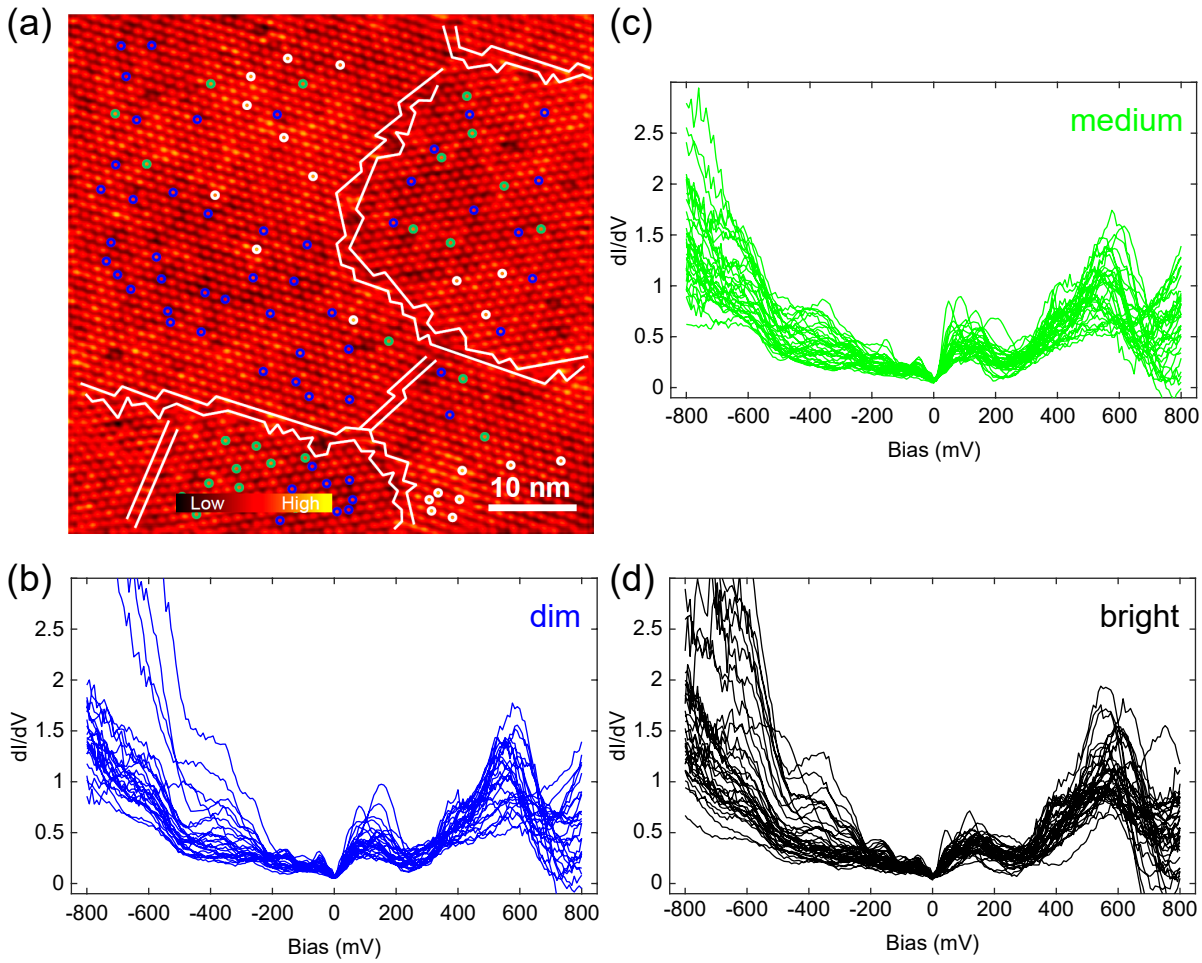

Figure 5: (a) The STM topographic image of 1 T-TaSSe taken at the area of 60 $\times$ 60 nm^2, with the scanning parameter at $V_s = +$ 800 mV and $I_t =$ 50 pA (the same image as Figure 1 (c) in the main text). (b)-(d) The STS spectra of the 1 T-TaSSe. The thick (thin) solid lines in black, green and blue color represent the averaged (individual) dI/dV spectra taken from the CDW maxima with bright, medium and dim brightness contrasts, which are indicated by the white, green and blue circles marked in (a), as classified in Figure S3.

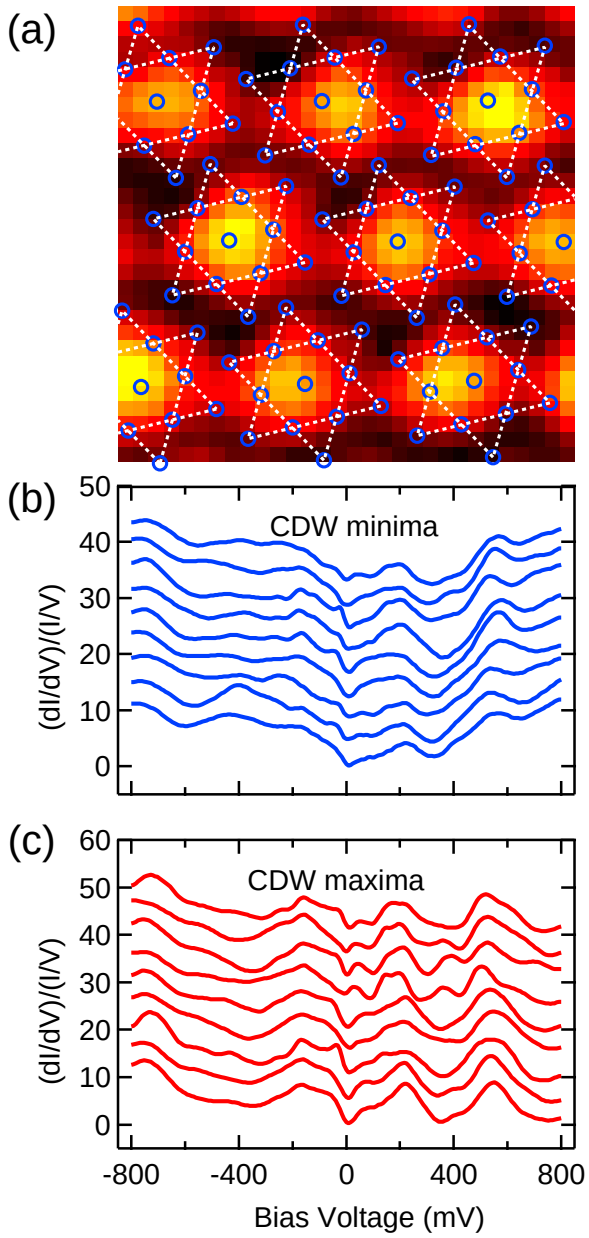

Figure 6: (a) The STM topographic image acquired with the area of 3.6×3.6 nm^2 during dI/dV measurements (V_s = - 800 mV and I_t = 900 pA). In total, dI/dV are measured on 900 points. The star of David pattern of the CDW structure is indicated. (b) and (c) display the normalized dI/dV spectra from the CDW maxima and minima regions, which are denoted by red and blue colors, respectively.

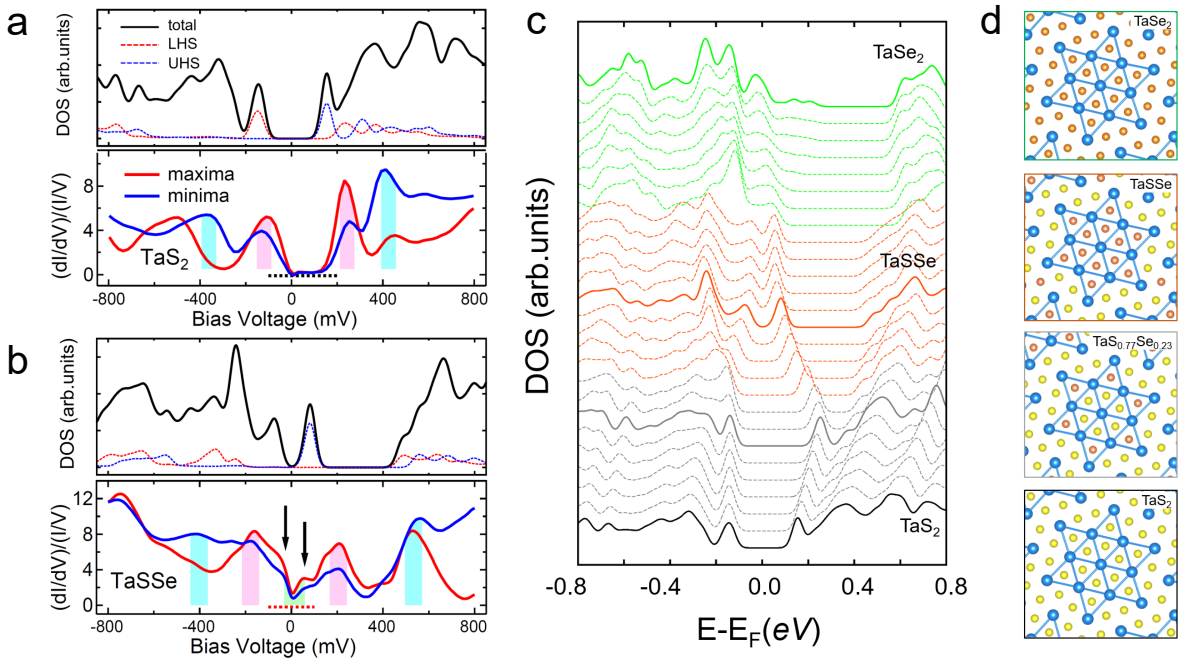

Figure 7: Theoretical density of states (DOS) and experimental dI/dV spectra of 1T-TaS_2 and 1T-$TaS_{2-x}Se_x$. (a) Theoretical DOS (upper panel) and experimental dI/dV spectra (bottom panel) of 1T-TaS_2. Red and blue lines are the spin-polarized local DOS ($\times 3$) at the center Ta atom of David star indicating the lower and upper Hubbard states, respectively. Black solid line denotes the total DOS. (b) Theoretical DOS (upper panel) of the lowest-energy TaSSe structure with the $\sqrt{13} \times \sqrt{13}$ unit cell. The bottom panel is the experimental dI/dV spectra of 1T-TaSSe. (c) Total DOS of the lowest-energy structures of 1T-$TaS_{2-x}Se_x$. (d) Selected atomic configurations.

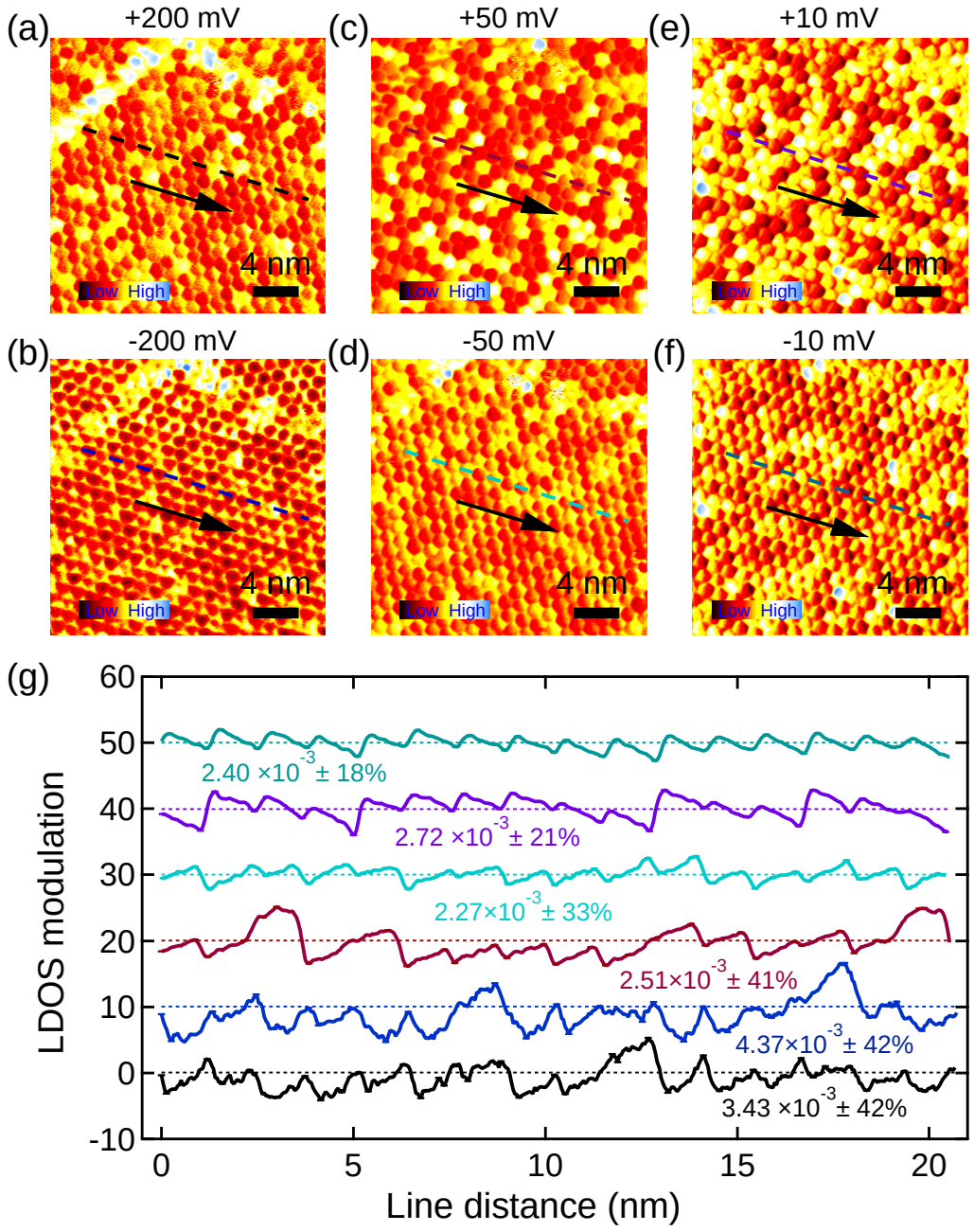

Figure 8: The LDOS maps were taken over the scanning area of 24×24 nm^2 at various sample bias of (a) V_s = + 200 mV, I_t = 50 pA; (b) V_s = - 200 mV, I_t = 50 pA; (c) V_s = + 50 mV, I_t = 50 pA; (d) V_s = - 50 mV, I_t = 50 pA; (e) V_s = + 10 mV, I_t = 50 pA; (f) V_s = -10 mV, I_t = 50 pA. (g) shows the spatial fluctuation of the electronic states along the dashed lines marked in (a)-(f). LDOS average values (arbitrary units) and their variational amplitudes in percentage are given.

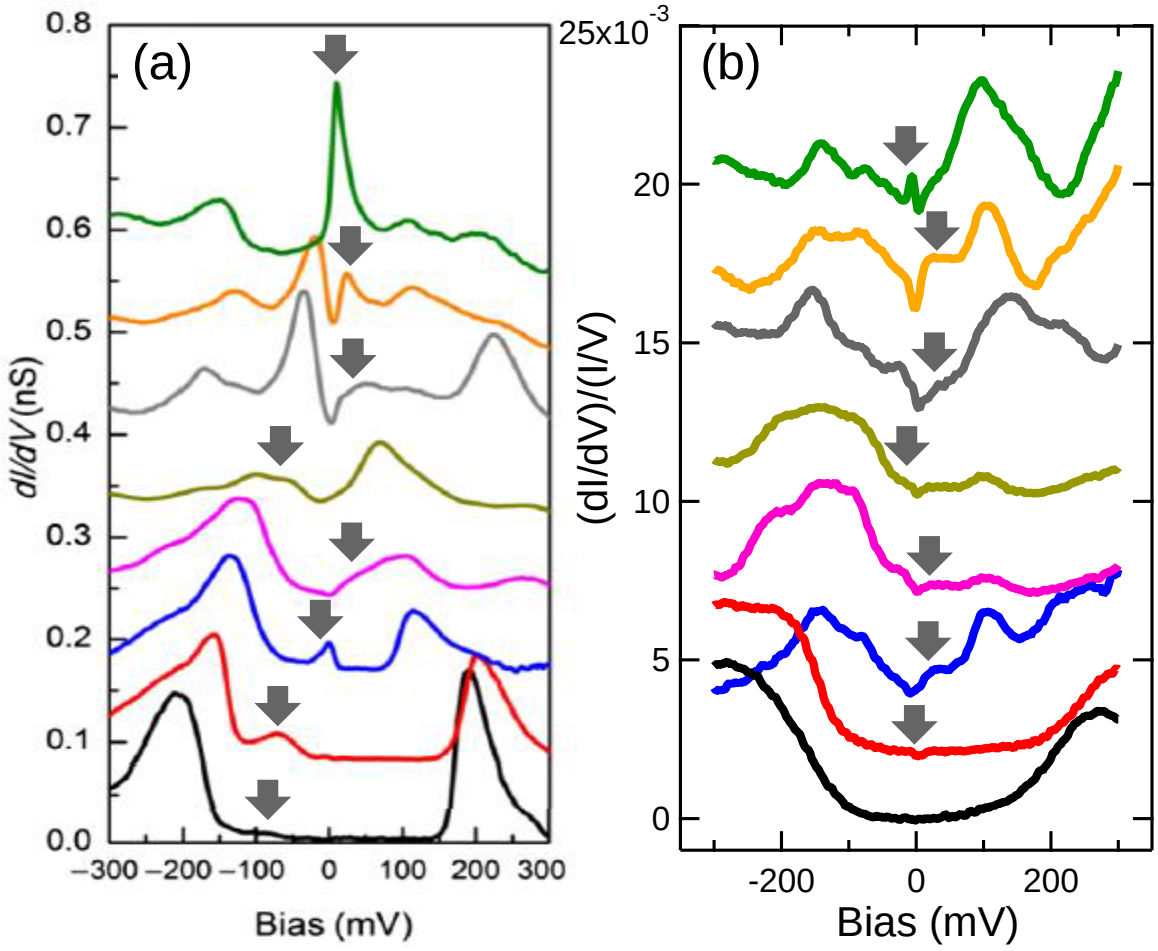

Figure 9: The local point STS spectra from (a) Ref.[3] and (b) the present data from various locations with different contrast. Most of the spectral features indicated by arrows were not explicitly mentioned in the previous work[3] but contribute to the pseudogap when they are averaged.

References

(1) Cho D.; Cho Y.-H.; Cheong S.-W.; Kim K.-S.; Yeom H. W. Interplay of electron-electron and electron-phonon interactions in the low-temperature phase of 1T-TaS_2, Phys. Rev. B 92, 085132 (2015).

(2) Smith N. V.; Kevan S. D.; DiSalvo F. J. Band structures of the layer compounds 1T-

TaS_2 and $2H$-$TaSe_2$ in the presence of commensurate charge-density waves. J. Phys. C: Solid State Phys. 18, 3175 (1985).

(3) Qiao S.; Li X. T.; Wang N. Z.; Ruan W.; Ye C.; Cai P.; Hao Z. Q.; Yao H.; Chen X. H.; Wu J.; Wang Y. Y.; Liu Z. Mottness collapse in $1T$-$TaS_{2-x}Se_x$ transition-metal dichalcogenide: An interplay between localized and itinerant orbitals. Phys. Rev. X. 7, 041054 (2017).

(4) Evers F.; Mirlin A. D.; Anderson transitions. Rev. Mod. Phys. 80, 1355 (2008).

(5) Richardella A.; Roushan P.; Mack S.; Zhou B.; Huse D. A.; Awschalom D. D.; Yazdani A. Visualizing critical correlations near the metal-insulator transition in $Ga_{1-x}Mn_xAs$. Science, 327, 665-669 (2010).

(6) Chhabra A.; Jensen R. V. Direct determination of the $f(\alpha)$ singularity spectrum. Phys. Rev. Lett. 62, 1327 (1989).